Mechanical Sonar Scanning Strategies for Fast Underwater Obstacle Detection on an Autonomous Surface Vessel

Lewis Luck[1,2], Ben Burgess-Limerick[2], Jen Jen Chung[1]

Abstract— Underwater obstacle detection is an increasingly necessary function of modern marine robotics, due to its important role in sub-surface collision avoidance in unknown environments. Mechanical scanning sonars (MSS) are affordable and accurate underwater sensors, that provide precisely controllable 360° coverage. However, MSS suffers from a slow sampling speed due to its single beam and mechanical actuation. To address this, this paper develops adaptive scanning strategies coupled tightly with a custom mapping and planning system to maximise information gain and collision response time on an autonomous surface vessel. The mapping system is demonstrated in field trials, and the scanning strategies are evaluated in simulation based on metrics of collision avoidance rate and smallest obstacle clearance. Results show our adaptive strategy increases the rate of intervention-free autonomous navigation by 70% in dense obstacle environments compared to an adaptation of a current state-of-the-art speed-adjusted strategy. Secondary findings suggest the adaptive strategy is also more robust across a range of obstacle reflection intensities and traversal speeds, and gathers more collision-relevant information from its surroundings than alternatives.

I. Introduction

Autonomous marine robotic systems are used widely across diverse applications including surveying, asset inspection, and defence. This work was conducted in collaboration with Pipar Automation, who were contracted by the Australian Institute of Marine Science (AIMS) to develop the ReefCat (Fig. 1), an autonomous surface vessel (ASV) for coral reef surveying on the Great Barrier Reef. This reef environment is representative of the challenging underwater environments common in autonomous marine systems, as it is coarsely mapped, irregularly shaped and constantly changing over time [1]. To maintain the safety of the ReefCat in this hazardous environment, underwater obstacle detection and collision avoidance is crucial.

For sub-surface sensing, sonar is necessarily used instead of visual or LiDAR sensors due to the high attenuation of electromagnetic radiation in water, a denser medium than air. Various sonar configurations are commonly used in collision avoidance, including multibeam forward-looking sonars (FLS) [2]–[4] and arrays of single-beam echosounders [5], [6]. However, the former can be prohibitively expensive, large and power-hungry for smaller or mass-produced vessels, and both configurations suffer from a significantly limited field of view. Instead, mechanical scanning sonars (MSS) are compact and affordable sensors that have been

[1] School of Electrical Engineering and Computer Science, The University of Queensland, Brisbane 4072, Australia, l.luck@student.uq.edu.au, jenjen.chung@uq.edu.au
[2] Pipar Automation, Spring Hill, Brisbane 4000, Australia.

Fig. 1: The ReefCat robotic platform.

widely used in autonomous systems [7]–[11] and offer omni-directional sensing by providing a single, 360° mechanically steerable acoustic beam. For these reasons, two Ping360 MSS from Blue Robotics were selected for the ReefCat.

One disadvantage of MSS are their slower update rate. For the Ping360, a full revolution of 400 equally spaced samples can take over 10 seconds, compared to 10Hz or higher update rates for multibeam sonars. This limitation provides a powerful motivation for the development of intelligent MSS scanning strategies to facilitate maximum information gain, which is as yet inadequately addressed in the literature. Despite studies referencing the need for an intelligent high-level controller for MSS [7], no dynamic strategy has been implemented to maximise the environmental information gathered for the time-critical sampling speeds of MSS. The dual MSS platform of ReefCat, shown in Fig. 2, is also unexplored in prior work and adds significant opportunity for complex, collaborative scanning strategies.

We address these gaps by developing an intelligent, adaptive scanning strategy based on a comprehensive view of the ASV obstacle avoidance problem. To achieve this, we present a probabilistic mapping implementation, inspired by prior work on sonar Bayesian occupancy maps [3], [5], [11],
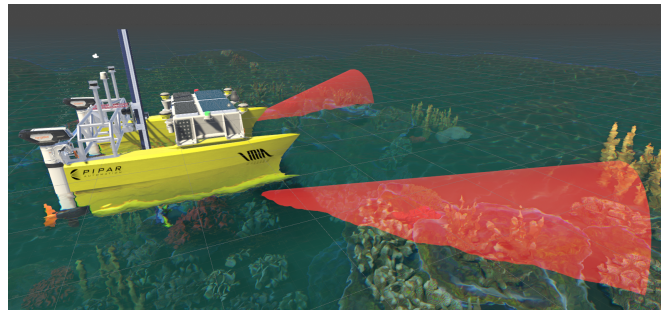

Fig. 2: Simulated ReefCat showing the dual MSS.

an ASV path planner and dual-MSS scanning strategies. Simulation and field test results validate our MSS scanning and mapping solution and demonstrate a 70% reduction in the rate of interventions (speed reductions required to avoid obstacles that were detected too late) when navigating dense obstacle environments.

II. Related Work

A. Mapping and Planning

Sonar sensors suffer from an imprecise propagation profile due to the mechanics of acoustic energy transmission. Sonar reflection returns are also prone to noise and influenced by several factors, including the turbidity of surrounding water, passive environmental disturbances, the angle of incidence of object surfaces and the porosity of the incident material [12]. Previous works overcome these limitations by using probabilistic approaches in mapping and planning that facilitate iterative updates and therefore greater accuracy over time.

The Bayesian occupancy grid is a common choice for mapping. Local Cartesian [3], [11] and polar [5] implementations are generally successful, as well as global Cartesian [7] mapping where precise localisation is available.

Probabilistic updates to these maps are dependent on translation from raw sonar returns (unsigned integer arrays representing the sonar 'intensities', or strength of reflection at each distance bin) to a probability of obstacle. Prior works typically translate raw returns into a range estimate using user-configurable thresholds [11], [13], [14]. Other approaches include setting a threshold to maintain a fixed false positive rate across all bins [3] or as the midpoint/minima of the bimodal distribution of reflection intensities [7], [15]. Cheng et al. [16] adds a second thresholding step, segmenting out water returns and noise alongside additional anomalies that have a large intensity difference from the sector average.

Villar et al. [17] apply a median filter to remove anomalous values (i.e. small spikes of high intensity noise). They also apply a per-scan adaptive local threshold instead of a fixed global threshold, which is more robust to variations in the reflections caused by changes in conditions or obstacles. The method steps iteratively through the reflection samples, computing the rolling median at each step, and flagging a detection when the next intensity return is more than double this rolling median.

Zhou et al. [18] address the angle-of-incidence ambiguity issue in sonar measurements by formulating a technique to isolate where in the wide-beam sonar propagation pattern a data return is most likely to come from using a 'dynamic inverse sonar model'. Thrun et al. [19] challenge the validity of the independent cell update assumption in occupancy maps, developing a 'forward sonar model' which considers each scan in its entirety to reduce the limitations of overlap between successive, conflicting wide-beam measurements. Grefstad et al. [11] combine both of these models to create a successful Bayesian grid for collision avoidance.

B. Scanning Strategies

A unique feature of the MSS compared to other sonars is its manoeuvrability: its position can be precisely controlled through software, and it can thus be directed through a large range of different scanning patterns [14], [15], [20]. Galarza et al. [10] select optimal MSS parameters for obstacle detection, opting for a range of 70m, a field of view of 90° and an angle resolution of 0.9° for their use case. These parameters are noticeably fixed, and not responsive to a changing environment as will be necessary for the Reefcat. Chen et al. [8] suggest a more dynamic approach using multiple different range setting parameters and switching between each as obstacles are found to trade off between speed of scan and accuracy.

Galarza et al. [10] also comment on the relationship between speed of scan, field of view and accuracy in obstacle detection. For their sonar and ASV moving at 1m/s, the 90° pattern takes 12 seconds to scan, during which time the ASV may move up to 12m, and thus be at risk of a new collision not previously identified at the start of the scan pattern. A more structured quantification of this relationship is presented in [7]. They frame the problem as a trade-off between ASV velocity and scanning speed, deriving an equation linking the two and discussing the resulting granularity of data returns (e.g. obstacles can appear suddenly if scanning slowly). This is a useful consideration and will be used as inspiration for the scanning strategy design of this paper.

III. Methods and Implementation

A. MSS Mapping Considerations

The Ping360 emits an irregular cone-like propagation pattern, with a vertical beamwidth of 25° and horizontal beamwidth of 2°. This transmission profile requires consideration before the design of the mapping system, as the vertical beamwidth causes measurement ambiguity across the depth axis of the ASV (measurements could equally come from above or below the sonar transducer). Therefore, the Ping360 may risk obstacle 'dropout'; that is, losing sonar-sight of an obstacle due to it falling beneath the propagation profile of the Ping360. However, due to the geometry of the ASV, it can be trivially shown that an obstacle which threatens the lowest point of the ReefCat (the sensing payload, 1.6m below the water surface), will only drop out of sight at 3.6m in front of the Ping360, which is less than a metre in front of the ReefCat due to the placement of the MSS towards the stern of the vessel. The indicative geometry of this scenario is illustrated in Fig. 3.

As any obstacle avoidance system should already have identified and evaded an obstacle this close, the Ping360 remains acceptable for use in collision avoidance. However, the depth ambiguity issue prompts use of a solely 2D 'birdseye-view' occupancy map. Probabilistic updates should also occur across the 2° horizontal beamwidth in a sector model, instead of a simplistic ray model, to ensure all possible obstacle reflections are acknowledged in the map.
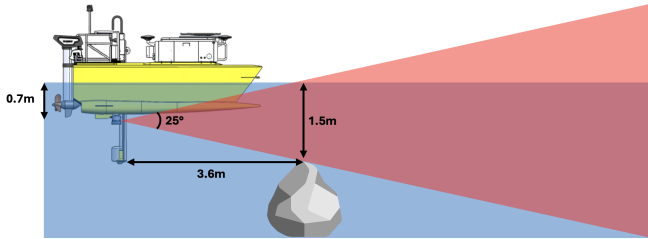
Fig. 3: Obstacle dropout problem.

B. Occupancy Grid Mapping: Practical Implementation

The mapping system for the ReefCat is constructed as a Bayesian occupancy map based on a square 2D global grid where each cell represents the probability of occupancy across a 12.5cm by 12.5cm square cell size (this size was selected to maintain floating point precision). Compared to AUVs that often have limited access to GNSS positioning due to the difficulty of reliable signal transmission through water, ASVs such as ReefCat have unobstructed views of the sky, and therefore optimal conditions for GNSS reception during typical operation. This is advantageous as it precludes the need for more complex localisation solutions such as underwater SLAM. The Septentrio AsteRx SBi3 Pro+ GNSS and INS positioning systems are employed on the ReefCat to provide centimetre-accurate localistation, allowing the construction of a global occupancy grid, which also greatly reduces complexity compared to local ASV-frame solutions.

The occupancy grid is segmented into arbitrarily sized 'tiles', selected at 10m by 10m for this implementation. This tiling system enables smaller computational and memory footprints for large surveying areas in which storing an entire rectangular map may be wasteful (e.g. a perimeter survey of a reef, which is a common use case). A simple coordinate-indexed map holds all tiles as floating point matrices (similar in form to images, enabling efficient processing), which are spatially referenced to a UTM origin for geo-located update, display and navigation operations. Note that tiles are stored discretely at fixed coordinate intervals, but at any time the mapping system will hold index ranges to these grids to create a local 'map-view' around the ReefCat's current position (selected as 100m by 100m, which is 320 cells by 320 cells), allowing simple updates on a single occupancy grid view. Fig. 4 demonstrates this tiled map composition during a field trial of the ReefCat, with the smaller occupancy tiles being generated as the ASV moves through its environment, and the map view (indicated in red) following it for real-time updates. Note that only tiles that are populated with a reading are stored in the map after they fall out of the map view for memory efficiency.

C. Probabilistic Updates from Sonar Returns

Raw sonar returns, packaged as an array of distance-binned intensities, are reported to this map-view (the local area around the ReefCat, geo-referenced globally). As previously described, the 2° horizontal beamwidth of these sonar returns necessitates a *sector* update for each sonar

Fig. 4: Demonstration of tiling and sector map design.

scan return, as opposed to a radial one. To achieve this, a fast sector traversal algorithm (using index-based iteration between two linear functions and a circular arc) is employed to step through the current incident sector of the sonar, based on the command angle and range of the MSS. For each cell in the sector, the Euclidean distance from the cell midpoint to the current GNSS location of the sonar is calculated. If this distance is less than the sonar exclusion distance (due to transducer ringing, the first 0.75m of samples are noisy and unusable), the cell is ignored. Otherwise, the maximum echo intensity corresponding to the cell midpoint distance plus or minus half the cell hypotenuse is found in the sonar returns array. This results in the scan being rasterised into a collection of cells in a sector shape, with each cell containing the maximum intensity from the raw return that falls inside the positional bounds that cell represents.

To convert these per-cell sonar measurements into an occupancy probability, an inverse sonar sensor model was found by experimental analysis and tuning. Field test observations showed some obstacles, like concrete bollards, were found to give consistently strong returns of over 150 out of 255 intensity, so the model was configured to always attribute a high update probability to such measurements. However, measurements of obstacles such as a river bank at high sampling ranges (i.e. 40m), were found to give reflection intensities as low as 30 out of 255, likely due to sheer angles of incidence and high absorptivity. Generally, objects at higher sample distances will result in lower reflection intensities, due to the large amount of energy that is lost into surrounding water from the cone-like propagation pattern of underwater acoustic transmission [12].

To address this range limitation, the sensor model biases the null probability with an inverse relationship to distance - that is, it attributes low intensities a lower probability of water at higher ranges. Additionally, preprocessing employs z-score outlier identification, inspired by [17], to magnify sharp rises in the spectrum at higher sample distances.

Raw sonar scans can also be optionally smoothed by median, Gaussian or discrete finite impulse respond filters to address noise caused by environmental conditions and water

turbulence (such as the wake of the ASV). The sensor model is also continuous across the 0-255 intensity range, instead of based on a fixed threshold. This creates a smoother update process to the map, especially in transition regions between low and high intensity where noisy measurements often sit.

D. Obstacle Detection and Planning

To register usable 2D polygon obstacles from the occupancy grid, a simple binary threshold is applied to the map based on a user-defined risk tolerance. The threshold used for this implementation was 0.8. Intuitively, this means 'register all obstacle cells which are 80% likely or more into polygons'. After this thresholding, a morphological closing is applied, to the resulting binary grid. Closing first dilates then erodes the region, and serves the purpose of filling in any small gaps/speckles in the masked obstacle grid cells. Finally, contour detection is performed using the Ramer-Douglas-Peucker algorithm for polygon simplification [21]. Polygons are stored as a list of their 2D vertices in counterclockwise order for registration, and are filtered by their area, calculated using Gauss' area formula (the 'shoelace method'). Any polygons with an area less than a minimum threshold, given as the size of two map cells for this implementation, is excluded from registration to remove small speckles in the map. Fig. 5 demonstrates this process in a noisy obstacle environment (a river bank and three concrete bollards), showing occupancy grid cells higher than 0.6 in orange/red and the resultant simplified obstacle polygons in green probability, overlaid on satellite imagery.

All cells in the current map view (100m by 100m range) are processed every 100ms for polygon registration. The current map view is a sufficient subset of the entire map, as only obstacles interfering in immediate navigation are important for path replanning purposes. Obstacles are then dilated by a safety-margin (set at 3m) such that planning can occur safely on just the visibility graph of obstacle vertices.

Combining these obstacle polygons and the current GNSS position and dynamic state of ReefCat, the Minimal Construct path planning algorithm [22] is used to generate a collision-free path to the next waypoint, as specified by mission control (i.e. a marine scientist). During deployment, paths are smoothed considering ReefCat dynamics (its maximal turning circle, etc.) to produce viable action plans for the motor controllers to execute.

Fig. 5: Obstacle registration from a noisy occupancy map.

E. Simple Scanning Strategies

The timing behaviour of the Ping360 is a crucial consideration in designing an effective scanning strategy. A comprehensive characterisation established the timing relationship:

$$t_s = 0.006M + 0.00142R + 0.0035 \tag{1}$$

where M is the angular delta to be moved, R is the sampled range, and t_s is the total time in seconds required to perform the command.

Considering this timing relationship, the period of a full revolution scan at 20m range takes 15 seconds. With the two sonars scanning scanning every gradian, 200 gradians out of sync, this results in a >7.5 second gap between either sonar looking in the direction of travel of the ReefCat. If travelling at 5 knots, its expected maximum speed, this results in a worst-case obstacle approach between sensing of over 19m, rendering a naïve revolution strategy inappropriate for collision avoidance.

Limiting the MSS to concentrate scanning in the forward direction of the ASV, which is where the chance of collision is most likely, can address this issue [7]. Ideally, this front-scanning sector should dynamically change based on speed. Intuitively, when the ASV is stationary or moving slower, it is allowable to cast in wider sectors to gather more information on surrounding obstacles, and when it accelerates, it should scan in narrower sectors to ensure it does not miss the approach of an obstacle from outside its field of view by too great a distance.

This concept can be formalised by designing a sector angular width formula that maintains a constant distance of obstacle approach:

$$w = \frac{dM}{vt_s}, \tag{2}$$

where w is the sector width in gradians, d is the constant obstacle approach distance, v is the current speed of the boat, t_s is the scan time for each scan of the sonar in seconds and M is the sonar step size in gradians. Decomposing t_s using Equation (1), there are thus three configurable parameters that define the sector width: R, M and d. A simple speed-adjusted strategy is designed using a fixed range of $R = 20$m and a conservative obstacle approach distance of $d = 1$m.

Sector scanning can be extended by considering the dual sonar configuration of the ReefCat. If both sonars are configured to a front-facing sector, significant redundant overlap occurs. Instead, a 'windscreen wiper' pattern is adopted, defined by a small overlapping region and a larger sector scan to each side. An indicative diagram of the beneficial difference between a sector and windscreen wiper strategy is shown in Fig. 6.

To define the sector width for the windscreen wiper
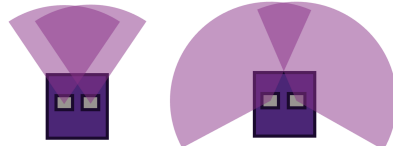
Fig. 6: Sector (left) vs. windscreen wiper (right) comparison.

approach, the sector is partitioned into three regions, as in Fig. 7, with the "overlap from front" region defined as f, followed by a width w and another duplicate f on the other edge of the sector.
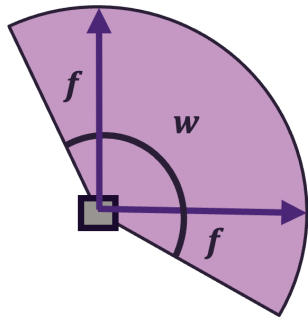

Fig. 7: Windscreen wiper sector partitioning diagram.

Fig. 8 demonstrates that only the angle w, not the entire width of $2f + w$, is travelled between the two sonars looking ahead: as one sonar beam is pointing ahead, the other is f in from the sector edge, and thus this other sonar beam next points ahead when the first sonar beam is f in from its sector edge. Therefore, w can be calculated the exact same as in Equation (2), and f can be set as a user parameter for the desired overlap, with the caveat that f must be at least $\frac{w}{2}$. The overlap f was defined to be a maximum of 10 gradians for this implementation.
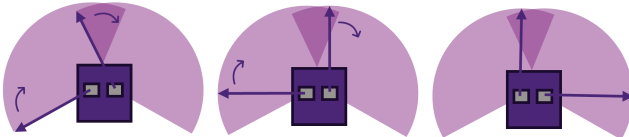
Fig. 8: Windscreen wiper example progression.

Fig. 9 plots the angular coverage of this speed-adjusted windscreen wiper strategy vs. speed-adjusted sector strategy across the speeds, v, for the ReefCat (1-6 knots), and across step sizes, M, of 1, 2 and 4, with fixed $f = 10$ gradians, $d = 1$m and range $R = 15$m. Evidently, the windscreen-wiper pattern provides significantly superior angular coverage.

Finally, as both Ping360s operate optimally at a constant acoustic frequency (750kHz), a dual sonar strategy should maintain maximal angular distance between the directions of each sound transducer to minimise interference. This intra-sector beam positioning is computed using angular interpolation; upon entry to a synchronised strategy, the relative position of the current scanning beam (left or right) which is closest to the front of the boat is found and the other sonar's beam is set to the same relative offset.
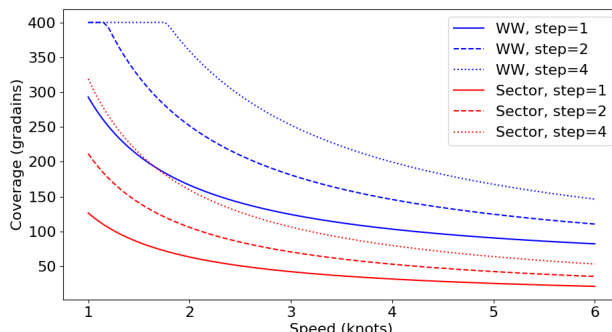
Fig. 10 is used as an illustrative example. Upon resuming a windscreen wiper strategy, the beams are out of sync, with the left at $50°$ relative position, and the right $100°$. The closest angle to forward, the right one, remains, while the left gets forced to the same relative position as the right to re-establish synchronisation.
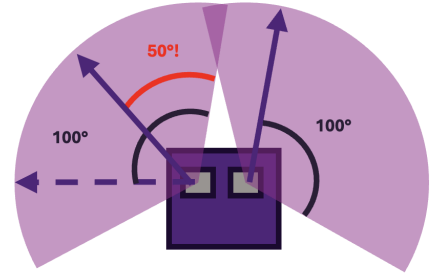
Fig. 10: Angular interpolation example.

Using this interpolation method, strategies adaptively respond to the real-time speed of ReefCat, narrowing at speed for faster front scan updates and expanding at slower speeds to collect more information from the environment.

F. Adaptive Scanning Strategy

Our adaptive strategy extends the speed-adjusted windscreen wiper by adding additional collision avoidance features. Firstly, the sonar sampling range (alongside sector width) is adjusted with speed. To this end, a new performance metric is introduced, the minimum response time, t_r. This metric defines how long the ASV should have to respond to an obstacle, and directly informs range, R, which can be trivially calculated as $R = t_r v$. This parameter t_r exists alongside the minimum obstacle approach distance, d, together these two parameters define the 'cautiousness' of the adaptive strategy.

By examining the responsiveness of the control system, a response time of $t_r = 10$ seconds was selected for this implementation. Fig. 11 demonstrates example illustrations of how windscreen wiper strategies may look under this new constraint, shrinking in sector width and growing in range as speed increases.

Secondly, an important consideration in marine obstacle avoidance is the irregular ocean environment. To address this, each scanning sector is centred on the course-over-ground direction vector (derived from the integrated localisation solution from the GNSS/INS unit) instead of simply the front of the ASV. This ensures the strategy is responsive to cross-current ocean conditions by biasing scanning in the true direction of travel, not just the ASV bearing.

Fig. 9: Angular coverage strategy comparison.
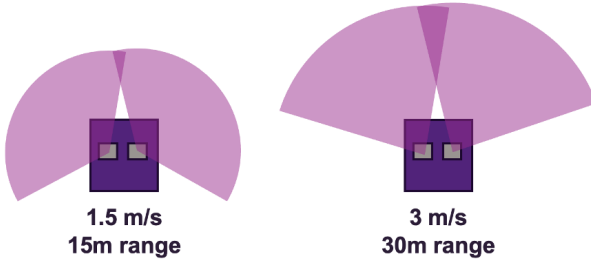
Fig. 11: Speed-dependent windscreen wiper sector and range.

One disadvantage of the speed-adjusted windscreen wiper strategy is the step size tradeoff: larger step sizes allow much greater angular coverage (Fig. 9), while smaller step sizes offer a more detailed and granular but width-limited scan.

This paper presents 'region-of-interest adaptive scanning' as a solution to this issue. This strategy employs a larger step size ($M = 4$) in a speed-adjusted windscreen wiper pattern during normal operation, and when it detects a 'region-of-interest', it proceeds to decrease step size (to $M = 1$) to repeatedly scan the region in greater detail. This ensures the strategy does not waste time scanning spaces known to be safe, instead scanning widely in unoccupied regions then concentrating detailed scanning in the places that need it, like obstacles. Repeated scanning of obstacles is particularly useful as often lower intensity returns that can originate from water noise, but which repeatedly in the same cell indicate an obstacle, will require multiple Bayesian updates to attain a high probability in the obstacle map.

Three regions of interest, pictured in Fig. 12, are identified as useful for the collision avoidance problem. When the strategy identifies any of the three region types, the wind-screen wiper pattern is interrupted, and one sonar (the one with the smallest angular travel time to the scan region) is diverted to iteratively scan the region while the other *covers* the front scan section using a speed-adjusted sector strategy. This ensures the ASV continues to have adequate direction-of-movement coverage while scanning regions in detail.

Firstly, *obstacles* that pose a collision risk are scanned in detail. The strategy will divert to iteratively scan a polar region if a scan is registered as 'useful'. An update to a cell in the occupancy map is defined as 'useful' information if it provides enough additive or subtractive information (defined by a user-configurable threshold). Additive information occurs when an update increases the probability of a cell by more than a threshold (selected as 0.05, to indicate a sufficiently significant probability update occurred) and is not yet registered as an obstacle (i.e. is below the obstacle probability threshold). Subtractive information refers to when a cell is already above the obstacle threshold, and the proba-

bility decreases in the Bayesian update. Additive information is useful when an obstacle needs to be updated quickly into the map, and subtractive information is useful to encourage iterative scanning to remove regions that were registered as obstacles and then appear as water (for example, turbulent water in the wake of the ReefCat) from the map. Algorithm 1 describes this heuristic computation process.
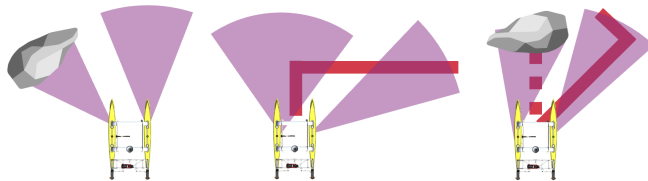
Algorithm 1 Additive and subtractive information updates.

1: **for** each cell $\in$ sector **do**
2:     **if** prior $< P_{\text{obs}}$ **and** posterior $-$ prior > 0.05 **then**
3:         $h_{\text{additive}} \leftarrow h_{\text{additive}} + 1$
4:     **end if**
5:     **if** prior $> P_{\text{obs}}$ **and** $P(\text{water}) > P(\text{obstacle})$ **then**
6:         $h_{\text{subtractive}} \leftarrow h_{\text{subtractive}} + 1$
7:     **end if**
8: **end for**

The obstacle-scanning pattern is also intelligently range limited. Using median outlier detection inspired by [17] an estimate for the range an obstacle lies within a scan is generated. The obstacle-scanning strategy changes its range at each scan update to this estimate, plus 5m to accommodate changes in the geometry of the obstacle. This saves time by not sampling unnecessary details behind an obstacle.

The adaptive strategy also focusses on regions-of-interest based on its path. Even adjusted for ocean conditions with a course-over-ground centring, the ASV will at best look in its direction of travel, but not in the direction it will soon be in if its approaching a turn. *Path aware scanning* address this issue by aborting any other current scanning (including obstacle-scanning, covering and normal windscreen-wiper states), and forcing one sonar to scan in the direction of the upcoming turn. It does so by iteratively computing the UTM point that corresponds to a certain distance along its path (set at 10m for this implementation). If the scan angle needed to point the MSS in the direction of this point diverges from the current course-over-ground by more than a difference threshold (set to 10 gradians), and is therefore not adequately covered by normal forward-scanning, the adaptive scanning strategy will divert the angularly closest sonar to scan that path point in a speed-adjusted sector pattern. Similar to the obstacle-scanning pattern, the other sonar will adopt a speed-adjusted sector to take over the 'covering' pattern looking in the forward direction.

Such an implementation ends up with two beneficial effects: (i) as the ASV approaches a pre-configured operator turn, it will start scanning in the direction it is about to turn; and (ii) if an obstacle appears in the path of the ASV and the path has to quickly change to avoid collision with the obstacle, the strategy will also immediately change its scanning pattern to look in the direction of the newly computed path. Both of these region-of-interest features are highly beneficial for collision avoidance, validating projected changes in the ASV path without needing to wait for the ASV to be close enough to the path point to naturally scan it in default forward scanning.

Fig. 12: Obstacle, turn and path recomputation regions of interest with forward-covering scanning (left to right).

IV. RESULTS AND DISCUSSION

A. Mapping

Fig. 13 demonstrates the success of the mapping system deployed to the ReefCat when navigating the Rivergate Marina on the Brisbane river. In general, the system clearly delineates obstacles and provide a sufficiently accurate representation of the environment for collision avoidance planning. Numerous sources of error can be present in mapping, for example erroneous returns from the turbulent wake of the ReefCat or sheer obstacles being interpreted as water due to the low intensity of their return. Both these issues were partially addressed by limiting the bounds of the occupancy map probability to between 0.05 and 0.95 (to avoid inappropriate high/low probabilities that are hard to quickly adjust), but future research is needed to effectively approach these error sources.

B. Scanning Strategies

For validation purposes, a high-fidelity simulation (Fig. 2) was developed in the Unity 3D game engine. The simulated ReefCat hull is rigged for accurate hull-fluid dynamics, computed using a physics engine interacting with a realistic ocean simulation supporting wave spectra and currents. Simulated digital-twin sensors (that use and output identical message packets as the real sensors) are also implemented for an effective end-to-end simulation of vehicle control to holistically evaluate the collision avoidance and navigation system. A Ping360 MSS simulator (accurate to the timing model in Equation (1)) was also developed, leveraging parallel raytracing across a dilated cone propagation profile with additive Gaussian noise and scaling reflection intensities by the incident angle of the ray hit for increased realism.

We compared our proposed adaptive scanning strategy (AS) against a naïve windscreen wiper strategy (NWWS), fixed at $100°$ width, and a speed-adjusted windscreen wiper strategy (SWWS) with a step of $M = 1$, with all other performance constants held as defined throughout Section III. Each method was evaluated in a set of 10 random dense
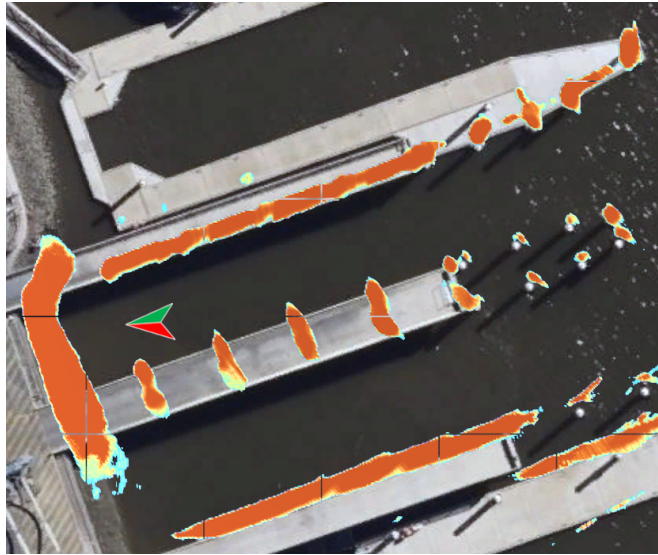
Fig. 13: Mapping field test in Rivergate Marina.
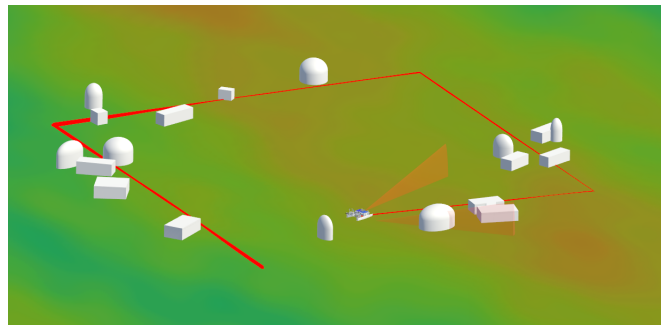
Fig. 14: Example random simulated obstacle course.

obstacle courses where the simulated ReefCat was directed to navigate a 200m path (Fig. 14).

Fig 15 shows an example of the path planner's output during navigation of such a obstacle course (a different one to 14). The true outlines of the obstacles can be seen in magenta, the scanned surfaces in red, the dilated boundaries of these obstacles in yellow and the generated straight line path in red. Note for simulation testing no path smoothing is applied.
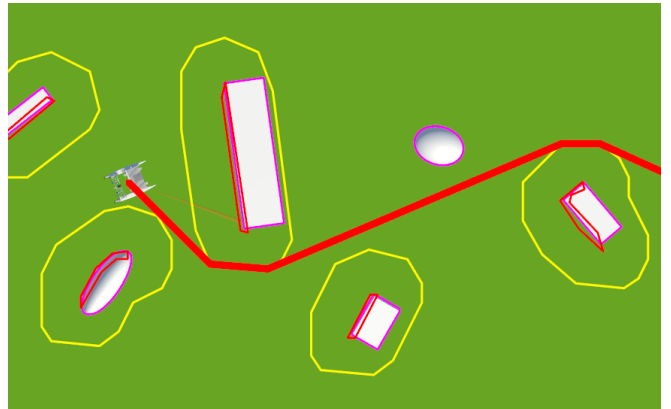

Fig. 15: Example path planning in simulation.

The main metric computed from each set of tests was the 'no-intervention rate'. Detecting obstacles early and accurately affords the planning system time to recompute the path and turn early, thereby allowing ReefCat to maintain a constant speed and complete a given path efficiently without unwanted decelerations. Therefore, a 'no-intervention' metric was recorded that indicates whether the ASV needed to slow down or stop to perform a collision avoidance manoeuvre.

Preliminary testing found NWWS performed poorly, with a no-intervention rate of 0.22. Therefore, more detailed analysis proceeded only for the other two strategies, including a comparison across multiple speeds (2, 4 and 6 knots) and reflection intensities (30, 50 and 80 out of 255). Varying the reflection intensity parameter varies the mean intensity of a simulated sonar return, (which is also adjusted by distance and angle-of-incidence through the MSS simulator) and aims to evaluate the robustness of the strategy to challenging scanning conditions.

Fig. 16 compares performance across multiple speeds and sonar reflection intensities, with each bar representing the rate over 10 randomly generated obstacle courses. AS outper-
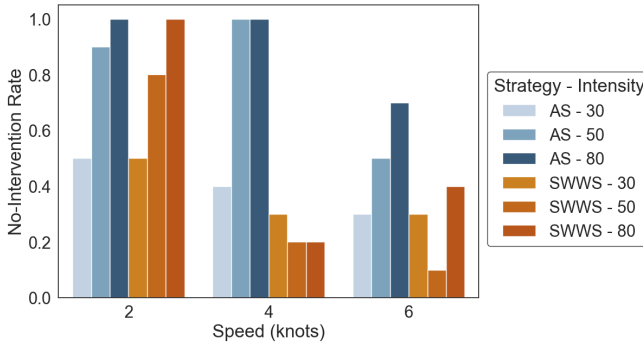
Fig. 16: No-intervention rate of adaptive and speed-adjusted windscreen wiper strategy across speeds and reflection intensities.

forms SWWS, both on average, with a mean no-intervention rate of 0.7 compared to 0.411 (70% improvement), and across all speeds and reflection intensity conditions. For lower speeds (2 and 4 knots) and high intensity (80 intensity), 100% collision avoidance was achieved with AS, while SWWS achieved 100% avoidance only for 2 knots and 80 intensity. In general, the SWWS had a significant quantity of its interventions from either a) not registering obstacles, particularly at low reflection intensities which requires multiple scans, fast enough and b) from too-late detection of obstacles when changing direction rapidly. The region-of-interest scanning of the AS addressed both these issues, leading to its outperformance.

Fig. 17 decomposes this no-intervention rate performance per random obstacle course, indicating the distribution is fairly well balanced with some outliers. Obstacle courses 3 and 7 appear to have been particularly difficult for both strategies, with only 0.1 no-intervention rate for the windscreen wiper and 0.6 or lower for the adaptive strategy. Despite this, again the adaptive strategy outperforms or matches the windscreen wiper in most cases, with the exception of obstacle course 8.
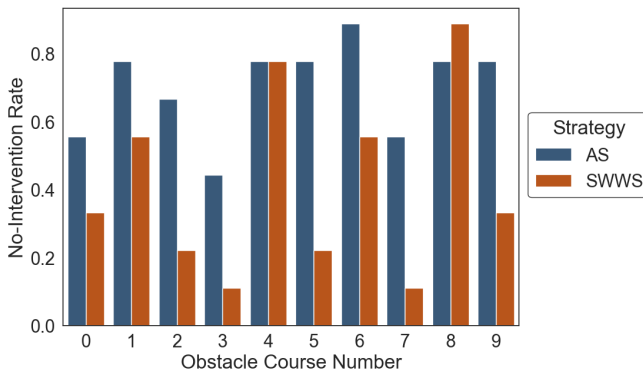
Fig. 17: No-intervention rate by obstacle course.

Table I shows the mean closest distance the ASV came to an obstacle averaged for the the trials that did not require intervention different speeds and intensities. Again the adaptive strategy outperforms, with an average of 0.26m additional clearance across speeds and 0.15m across intensities.

Mean clearances are about 1.3m in the most successful avoidance, which given the 2m beam of the boat and the 3m

dilation factor set for obstacles is a reasonably successful result. Additionally, these quantitative results reflect intuitive trends also observable in Fig. 16: an increase in speed results in a decrease in collision performance (faster navigation means less time to scan and register obstacles), and an increase in reflection intensity results in an increase in performance (easier-to-scan obstacles can be avoided earlier).

Closest Obstacle Distance (m)		
Speed (knots)		
2	4	6
AS	1.28	1.45	1.08
SWWS	1.04	1.01	0.88
Obstacle intensity		
30	50	80
AS	0.72	1.34	1.43
SWWS	0.75	1.28	0.99

TABLE I: COMPARISON OF CLOSEST OBSTACLE DISTANCE FOR EACH SCANNING STRATEGY UNDER DIFFERENT OPERATING CONDITIONS.

C. Obstacle Map Completion as Information Gain

A histogram of the information gain metrics for both strategies is presented in Fig. 18. Information gain was defined as the birds-eye-view ratio of the registered obstacles area compared to the ground truth obstacle area–the greater the information gain, the higher proportion of available obstacle information was registered into the map. Note this information gain metric was only computed for sets of given speeds and intensities where both strategies successfully completed the obstacle course without intervention: trials that stop early will inherently see less of the map and therefore are not a fair comparison.

In general, the adaptive strategy distribution is skewed higher than the speed-adjusted windscreen wiper distribution, though not by an overly significant margin. The mean is 17.83% for AS, and 15.46% for SWWS. AS had a maximum information gain of 34.1%, and a minimum of 4.9%, while SWWS had a maximum information gain of 25.6% and a minimum of 3.3%.

The greatest difference for a single trial was for Obstacle Course 6 at 80 intensity and a speed of 6 knots, where
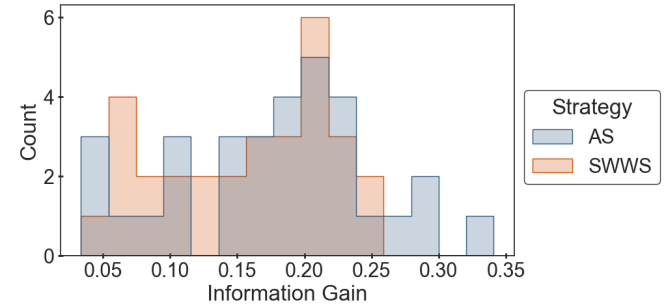

Fig. 18: No-intervention information gain comparison.

AS and SWWS attained 31.4% and 17.4% information gain respectively. Fig. 19 indicates a section of this course after both strategies navigated through it. Red polygons represent the obstacles registered from simulated scanning, and magenta represent the true outlines of the randomly generated obstacles (the white simulated 3D shapes). The information gain heuristic is therefore defined as the sum of the red polygon area divided by the sum of the magenta polygon area. Observing the top figure, AS registered a significantly greater quantity of the true information, represented as the abundance of red polygons on the edges of most obstacles, compared to SWWS on the bottom.
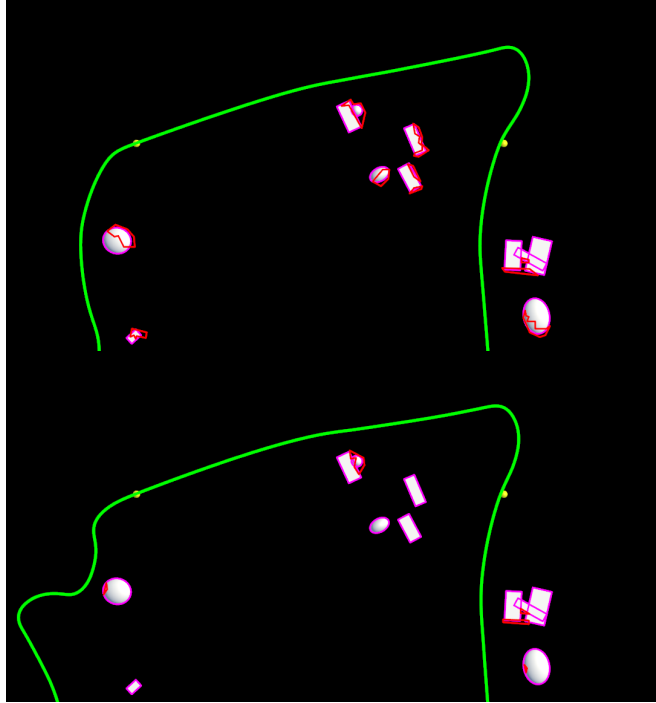
Fig. 19: Information gain example strategy comparison. Top: adaptive strategy. Bottom: speed-adjusted windscreen wiper strategy.

These results are consistent with the design intention; the adaptive strategy gathers more information from its surroundings than alternatives due to its broader angular coverage, and is also more likely to be able to register more of an obstacle due to its obstacle-scanning strategy, especially in low-intensity environments.

D. Failure Cases

Fig. 20 depicts the AS failing (requiring a deceleration intervention) on Obstacle Course 7. This is representative of a common issue–similar to SWWS, AS is susceptible to fail on complex areas of the path such as sharp turns. This contributed to Obstacle Courses 3 and 7, which had obstacles closest to path turns, being the lowest performing courses.

Despite the AS specifically targeting path-aware scanning through scanning preemptively on turns and path recomputation, the *quality* of the path the strategy based these scans on was low. The key issue was that the path published to the scanning strategy was a *straight-line* path between waypoints
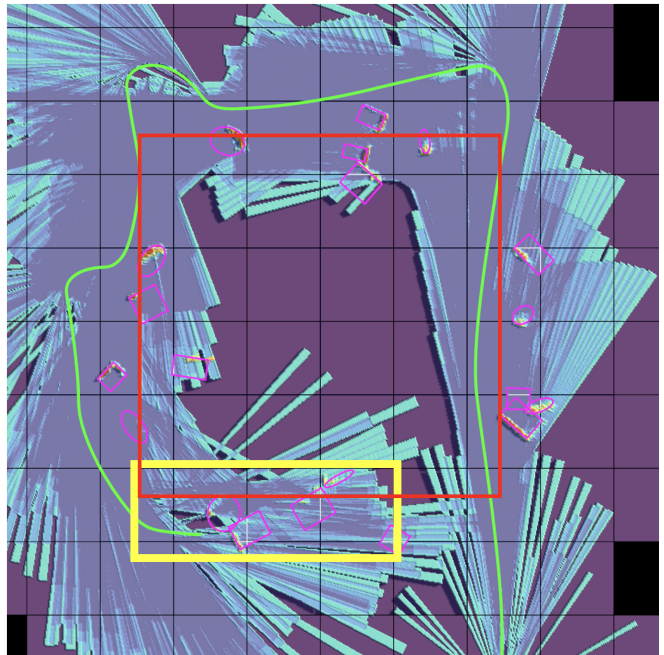

Fig. 20: Demonstration of complex path issue for AS.

and therefore unrealistic given the (simulated or real) vessel dynamic. In Fig. 20, this is represented in red, while the green line represents the trajectory of the ASV. Evidently, as the ASV approached the bottom left turn of the straight-line path, it successfully scanned in detail the straight-line waypoint path (note the densely updated region in the top of the yellow box), but it failed to scan where it actually ended up on its non-holonomic turning path (where the green line ends, indicating intervention was required).

This also explains an anomalous speed relationship discernible in the results - in some cases, contradictory to the intuitive trend, the AS performed *worse* at slower speeds. For example, AS required intervention to navigate Obstacle Course 3 at 2 knots, but did *not* for the same course at 4 knots. It also on average had a slightly lower clearance distance for 2 knots (1.285m) then 4 knots (1.36m). This is because at faster speeds, the forward-directed 'cover' scanner turns into scanning the obstacles faster, which is then sometimes able to register the obstacles that the path scanner missed by looking at an unrealistic straight-line path.

More accurate non-holonomic, dynamic path-planning, such as that being rolled out in the ReefCat sea trials, would greatly assist the scanning strategy in addressing both these issues and being able to scan the regions in turn that the ASV is most likely to navigate through.

Additionally, this issue exposes that the strategy does not adequately handle *two* competing regions-of-interest at once. That is, when a path recomputation or turn scan *also* finds an obstacle, the controller will default to path scanning behaviour, which is wide and less targeted than obstacle scanning, resulting in more time wasted. A more complex 'tri-state controller' that can adequately trade off the responsibilities of path scanning, obstacle scanning and 'covering' (scanning in front in the direction-of-movement) at once would likely improve results.

V. Conclusion

This work implemented a mapping and planning system for the ReefCat ASV, and presented an adaptive scanning strategy for the onboard MSS to improve autonomy outcomes. Probabilistic mapping which holistically considered the sonar-based collision avoidance problem was developed using continuous, distance-adjusted and sector-aware Bayesian updates on a tile-based occupancy map. Through the execution of field experiments on the Brisbane river, we showed that the resulting occupancy maps were qualitatively accurate to satellite imagery. We extended existing sonar scanning strategies to a dual sonar ASV platform through the speed-adjusted windscreen wiper, and developed a novel adaptive scanning strategy, coupling planning, mapping and sensing tightly for improved collision avoidance outcomes. Our adaptive strategy was shown to significantly outperform alternatives, achieving a 70% improvement in required interventions, more robust performance across sonar return intensities and ASV speeds, and greater environmental information gain than the speed-adjusted windscreen wiper.

The ongoing collection of quantitative data from ReefCat sea trials, especially on a real reef environment, will enable validation of the proposed system in future work. Using this data to develop non-holonomic and probabilistic local trajectory prediction will improve path-aware scanning, as discussed in relation to Fig. 20.

Additionally, further consideration of the dynamic reef and ocean environment, such as adaptively changing system parameters based on ocean state could provide a more robust and responsive system. For example, the obstacle dilation factor, response time and constant obstacle approach distance could all be increased in the presence of strong waves or currents that decrease the reliability of the ASV control system. Waves, which were demonstrated to be a capability of the ASV simulation but not directly tested in experiments, could then be incorporated as an additional design criteria for all scanning strategy comparisons.

Finally, the development of a previously discussed tri-state controller, which could dynamically prioritise path, obstacle and front direction scanning is also a key focus of future work. A more general extension of such a controller is a system framework that is generically optimisable for arbitrary cost/reward functions specified to it. Given such functions, which for example may periodically reward looking in the direction of travel, less periodically reward looking to the side and reward scanning on obstacles or noise proportional to the information gain such scanning may deliver, the framework would use optimisation theory to find the set of angle trajectories that optimise its information rate - the amount of useful information it gathers per second. Further exploration of such a strategy is arguably one of the most important suggestions for future work, as it generalises scanning and therefore makes the strategy more dynamic to different competing interests and complex obstacle environments.

References

[1] R. Beaman, "Ausbathytopo (great barrier reef) 30m 2017 - a high-resolution depth model (20170025c)," Canberra, 2017. [Online]. Available: http://dx.doi.org/10.4225/25/5a207b36022d2

[2] M. Franchi, A. Bucci, L. Zacchini, E. Topini, A. Ridolfi, and B. Allotta, "A probabilistic 3d map representation for forward-looking sonar reconstructions," in *IEEE/OES Auton. Underwater Veh. Symp.*, 2020.

[3] V. Ganesan, M. Chitre, and E. Brekke, "Robust underwater obstacle detection for collision avoidance," *Auton. Robots*, vol. 39, 10 2016.

[4] E. Galceran, V. Djapic, M. Carreras, and D. P. Williams, "A real-time underwater object detection algorithm for multi-beam forward looking sonar," *IFAC Proc. Volumes*, vol. 45, no. 5, pp. 306–311, 2012.

[5] C. Morency, D. J. Stilwell, and S. T. Krauss, "Use of a low-cost forward-looking sonar for collision avoidance in small AUVs, analysis and experimental results," arXiv preprint arXiv:2309.05785, 2023.

[6] R. Passarella, A. Zarkasi, H. Maghfur, . Sutarno, K. Exsaudi, A. Prasetyo, and H. Veny, "Autonomous surface vehicle (ASV) obstacle avoidance using Fuzzy Kohonen Network (FKN)," *IOP Conf. Ser.: Materials Sci. and Eng.*, vol. 648, p. 012023, 10 2019.

[7] H. K. Heidarsson and G. S. Sukhatme, "Obstacle detection and avoidance for an autonomous surface vehicle using a profiling sonar," in *IEEE Int. Conf. on Robot. and Autom.*, 2011, pp. 731–736.

[8] J. Chen, W. Pan, Y. Guo, C. Huang, and H. Wu, "An obstacle avoidance algorithm designed for USV based on single beam sonar and fuzzy control," in *IEEE Int. Conf. on Robot. and Biomimetics*, 2013, pp. 2446–2451.

[9] F. J. Solari, A. F. Rozenfeld, S. A. Villar, and G. G. Acosta, "Artificial potential fields for the obstacles avoidance system of an AUV using a mechanical scanning sonar," in *IEEE/OES South American Int. Symp. on Ocean. Eng.*, 2016, pp. 1–6.

[10] C. Galarza, I. Masmitja, J. González, J. Prat, S. Gomariz, and J. Del Rio, "Design obstacle detection system for AUV Guanay II," in *Int. Workshop on Mar. Technol.*, 2015, pp. 15–18.

[11] Ø. Grefstad and I. Schjølberg, "Navigation and collision avoidance of underwater vehicles using sonar data," in *IEEE/OES Auton. Underwater Veh. Workshop*, 2018, pp. 1–6.

[12] J. Marage and Y. Mori, *Sonar and Underwater Acoustics*. Wiley-ISTE, 2010.

[13] D. Horner, A. Healey, and S. Kragelund, "Auv experiments in obstacle avoidance," in *Proceedings of OCEANS 2005 MTS/IEEE*, 2005, pp. 1464–1470 Vol. 2.

[14] D. Ribas, P. Ridao, J. D. Tardós, and J. Neira, "Underwater slam in man-made structured environments," *J. of Field Robot.*, vol. 25, no. 11-12, pp. 898–921, 2008.

[15] Y. González, G. Oliver, and A. Burguera, "Underwater scan matching using a mechanical scanned imaging sonar," *IFAC Proceedings Volumes*, vol. 43, no. 16, pp. 377–382, 2010, 7th IFAC Symposium on Intelligent Autonomous Vehicles.

[16] C. Cheng, C. Wang, D. Yang, W. Liu, and F. Zhang, "Underwater localization and mapping based on multi-beam forward looking sonar," *Front. Neurorobot.*, vol. 15, p. 801956, 2021.

[17] S. A. Villar, F. J. Solari, B. V. Menna, and G. G. Acosta, "Obstacle detection system design for an autonomous surface vehicle using a mechanical scanning sonar," in *2017 XVII Workshop on Information Processing and Control (RPIC)*, 2017, pp. 1–6.

[18] M. Zhou, R. Bachmayer, and B. deYoung, "Mapping for control in an underwater environment using a dynamic inverse-sonar model," in *OCEANS 2016 MTS/IEEE Monterey*, 2016, pp. 1–8.

[19] S. Thrun, "Learning occupancy grid maps with forward sensor models," *Autonomous Robots*, vol. 15, no. 2, pp. 111–127, Sep 2003.

[20] H. Baek, B. H. Jun, and M. D. Noh, "The Application of Sector-Scanning Sonar: Strategy for Efficient and Precise Sector-Scanning Using Freedom of Underwater Walking Robot in Shallow Water," *Sensors (Basel)*, vol. 20, no. 13, Jun 2020.

[21] D. Douglas and T. Peucker, "Algorithms for the reductions of the number of points required to represent a digitised line or its caricature," *The Canadian Cartographer*, vol. 10, no. 2, pp. 112–122, 1973.

[22] M. Missura, D. D. Lee, and M. Bennewitz, "Minimal construct: Efficient shortest path finding for mobile robots in polygonal maps," in *2018 IEEE/RSJ International Conference on Intelligent Robots and Systems (IROS)*, 2018, pp. 7918–7923.